

RESEARCH

Open Access



FROP-1 peptide-conjugated ultrasmall superparamagnetic nanoparticles as a targeted T1-weighted MR contrast agent for breast cancer: in vitro study

Melika Samari^{1,2}, Zahra Alamzadeh¹, Rasoul Irajirad¹, Abolfazl Sarikhani^{1,2}, Vahid Pirhajati Mahabadi³, Habib Ghaznavi^{4*} and Samideh Khoei^{1,2*}

Abstract

Background The aim of this study was to produce ultrasmall superparamagnetic iron oxide (USPIO) nanoparticles (NPs) conjugated to the FROP-1 peptide for targeted magnetic resonance imaging (MRI) of breast cancer cell lines and to evaluate its application as a specific and targeted T1-weighted MR imaging contrast agent in vitro. Sodium citrate-stabilized Fe₃O₄ NPs were conjugated with the FROP-1 peptide by 1-ethyl-3-(3-dimethylaminopropyl) carbodiimide hydrochloride (EDC) to form a novel Fe₃O₄@FROP-1 specific target contrast agent. The specificity and targeting of Fe₃O₄@FROP-1 to bind FROP-1 receptors were investigated in vitro by cellular uptake and cellular MR imaging.

Results In this study, the synthesis of water-soluble ultrasmall Fe₃O₄ NPs was performed by the co-precipitation method. XRD, TEM, and VSM analyses showed the formation of the Fe₃O₄ NPs with an average size of about 3.78 ± 0.2 nm. FT-IR spectroscopy approved the conjugation of the FROP-1 peptide with the Fe₃O₄ NPs. The synthesized Fe₃O₄@FROP-1 NPs showed good biocompatibility, and the high r1 relaxivity and r2/r1, respectively, were 2.608 mM⁻¹s⁻¹ and 1.18. The biocompatibility of the Fe₃O₄ and Fe₃O₄@FROP-1 NPs on the MCF-7, SKBR-3, MDA-MB-231, and MCF-10 cell lines was determined using cytotoxicity analysis. The specific targeting effect on the cells was verified by in vitro cellular uptake and cell MR imaging.

Conclusion It was found that the contrast intensity of the Fe₃O₄@FROP-1 nanoprobe increases as Fe concentration increases. Cellular uptake of the Fe₃O₄ and Fe₃O₄@FROP-1 NPs was quantified using ICP-MS. The synthesized NPs had better imaging performance than Dotarem (gadoterate meglumine). The findings showed that Fe₃O₄@FROP-1 NPs have potential utility as a specific and targeted T1-weighted contrast agent in breast cancer MR imaging.

Keywords T1-weighted MRI, Breast cancer, Molecular imaging, FROP-1 peptide, SPIONs

*Correspondence:

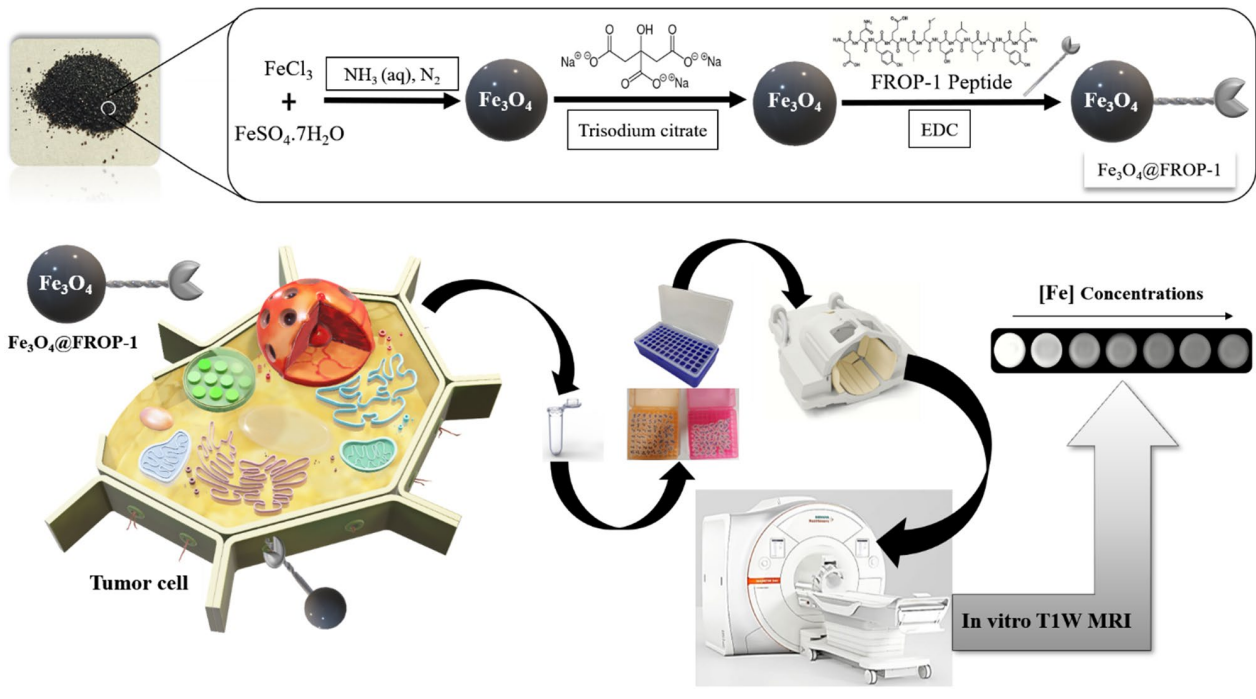
Habib Ghaznavi
dr.ghaznavi@zaums.ac.ir
Samideh Khoei
khoei.s@iums.ac.ir

Full list of author information is available at the end of the article



© The Author(s) 2025. **Open Access** This article is licensed under a Creative Commons Attribution-NonCommercial-NoDerivatives 4.0 International License, which permits any non-commercial use, sharing, distribution and reproduction in any medium or format, as long as you give appropriate credit to the original author(s) and the source, provide a link to the Creative Commons licence, and indicate if you modified the licensed material. You do not have permission under this licence to share adapted material derived from this article or parts of it. The images or other third party material in this article are included in the article's Creative Commons licence, unless indicated otherwise in a credit line to the material. If material is not included in the article's Creative Commons licence and your intended use is not permitted by statutory regulation or exceeds the permitted use, you will need to obtain permission directly from the copyright holder. To view a copy of this licence, visit <http://creativecommons.org/licenses/by-nc-nd/4.0/>.

Graphical Abstract



Background

Accurate and early detection of breast cancer is a very important and vital category. Although current diagnostic methods do not directly prevent metastasis and mortality, they play a crucial role in early detection and facilitating timely and effective treatment planning, which can improve patient outcomes. Have targeted agents been effective in creating a specific diagnostic method? To what extent have diagnostic imaging techniques been successful in diagnosing breast cancer early and accurately? These are some of the questions that are often asked in the field of diagnosis and improvement of its methods. Early and accurate diagnosis of cancer plays an important role in choosing the appropriate treatment as well as successful treatment and prevents metastasis and death.

Despite the recent significant advances in the diagnosis and targeted treatment of breast cancer, this disease is still known as the second most common cancer in the world, with a high risk of metastasis and mortality among women [1, 2]. The inherent heterogeneity of breast tumors makes accurate and early diagnosis and prognosis, as well as choosing the appropriate treatment method, challenging [3, 4].

Nowadays, MRI is known as one of the most powerful and widely used non-invasive imaging methods due to the production of images with high spatial resolution and the ability to access 3D tomographic information

from soft tissues, including tumors [5, 6]. However, the relatively low inherent sensitivity of this technique limits accurate and non-invasive tumor detection. Currently, in most MRI examinations, contrast agents are used to increase sensitivity and improve image contrast. In general, MRI contrast agents are classified into T1-weighted (T1w) and T2-weighted (T2w) depending on their size or distribution in the body, magnetic properties, and the effect they have on image contrast [7, 8]. Contrast agents T1 and T2 improve image contrast by reducing longitudinal (T1) and transverse (T2) relaxation times, respectively [9]. T2 contrast agents have a high intrinsic sensitivity, which creates a long-range and heterogeneous magnetic field. Due to the heterogeneous magnetic field caused by paramagnetic or diamagnetic materials, the signal intensity decreases and distorts the background image. This phenomenon is known as the MRI “blooming effect”, or the intrinsic dark signal of T2w, which causes signal loss and background image distortion, making precise localization of the contrast agent challenging [10, 11]. In MRI blooming effect, the size of an object measured in the MR image is larger than its real size. Due to the blooming effect as well as the presence of other hypointense areas arising from metal deposits, calcification, and bleeding, the exact position of T2 contrast agents cannot be easily identified [12]. In contrast, the use of the enhanced T1 contrast improves imaging, distinguishes between different tissues, and avoids the blooming effect,

making them a preferred choice for clinical applications [13]. Gadolinium-based contrast agents (GBCAs) are commonly used as T1 contrast agents for clinical cancer imaging [11]. On the other hand, they cause lethal nephrogenic systemic fibrosis and accumulation in the brain [13], which has been warned about by the Food and Drug Administration (FDA) [12, 14].

USPIO NPs with high magnetic strength, safety, and good biocompatibility [15], have emerged as promising T1 contrast agents. Unlike conventional SPIONs, they do not affect the magnetic homogeneity or the background and also provide the possibility to determine the exact position of the contrast agent [16]. The optimal contrast agent T1 is the contrast agent in which r_1 is large and the ratio r_2/r_1 is small, while in the optimal contrast agent T2, the value of r_2 must be much larger than the value of r_1 [9]. However, these contrast agents are non-specific and cannot distinguish tumor invasiveness or produce effective, detectable contrast in small tumors and micrometastases. To address this challenge, targeted molecular imaging strategies have emerged as a promising approach. Peptides become target molecules due to their high specificity, high binding affinity, very small size, low toxicity, and acceptable stability [14, 17]. In 2007, the FROP-1 peptide was identified through a phage display system by Zitzmann et al. [18]. The 12-amino acid peptide FROP-1 [19] was labeled with ^{125}I and ^{131}I and evaluated for targeting, stability, and ability to bind to different types of cancer cell lines. The results showed that the highest uptake of the labeled peptide was related to the MCF-7 breast cancer cell and the thyroid cancer cell FRO82-2 [18, 20]. Despite its promising tumor-targeting ability, FROP-1 has not been investigated for MRI contrast enhancement, leaving a gap in the development of targeted molecular imaging approaches.

Although various MRI contrast agents have been investigated, the conjugation of USPIOs with a tumor-specific peptide like FROP-1 for targeted T1-weighted imaging remains unexplored. This study aims to develop a targeted T1 MRI contrast agent by conjugating FROP-1 peptide to USPIO NPs, synthesized by using the coprecipitation method and stabilized with sodium citrate. This conjugation is expected to enhance selective tumor targeting by improving nanoparticle uptake at breast cancer cell surface receptors. Unlike conventional GBCAs, which pose risks of toxicity and brain accumulation, or untargeted USPIOs with limited specificity, our approach offers improved specificity, contrast enhancement, and safety. To evaluate the efficacy of this targeted contrast agent, we characterize the synthesized Fe_3O_4 and $\text{Fe}_3\text{O}_4@$ FROP-1 NPs, assessing their magnetic performance, relaxivity, specific absorption, cytotoxicity, as well as T1w image signal intensity in breast cancer cells. In other words, targeted delivery of USPIO NPs conjugated to

the FROP-1 peptide in vitro as a T1w contrast agent can increase the sensitivity and specificity of MR imaging by facilitating their accumulation in breast cancer cell lines.

Materials and methods

Materials

Ferric chloride ($\text{FeCl}_3 \cdot 6\text{H}_2\text{O}$), ferrous chloride ($\text{FeCl}_2 \cdot 4\text{H}_2\text{O}$), sodium hydroxide, sodium citrate, ethylene diaminetetraacetic acid (EDTA), hydrochloric acid, and dimethylsulfoxide (DMSO) were purchased from Kelong Chemical Co. (Chengdu, China, AR). Pluronic F127 (F127) was purchased from Sigma-Aldrich (Shanghai, China). 1-Ethyl-3-[3-(dimethylamino) propyl] carbodiimide hydrochloride (EDC), N-hydroxysuccinimide (NHS), and 2-(N-morpholino) ethanesulfonic acid were purchased from Aladdin (Shanghai, China). A 12-amino acid FROP-1 peptide ($\text{Glu}^1\text{-Asp}^2\text{-Tyr}^3\text{-Glu}^4\text{-Leu}^5\text{-Met}^6\text{-Asp}^7\text{-Leu}^8\text{-Leu}^9\text{-Ala}^{10}\text{-Tyr}^{11}\text{-Leu}^{12}$) (M.W. 1485.7 Da) was purchased from HUICHEM (Shanghai Huirui Chemical Technology) Co., Ltd. (Shanghai, China). Dulbecco's Modified Eagle's Medium (DMEM) were purchased from GIBCO (Invitrogen, Germany). Trypsin-ethylenediaminetetraacetic acid (EDTA) and penicillin-streptomycin solution was purchased from Sigma-Aldrich Corp. (St Louis, MO, USA). The MCF-7, SKBR-3, MDA-MB-231 (human breast cancer), and MCF-10 (normal) cells were purchased from the Pasteur Institute of Iran (Tehran, Iran) and cultured separately.

Synthesis of the Fe_3O_4 and $\text{Fe}_3\text{O}_4@$ FROP-1 NPs

The synthesis of uniform and ultrasmall Fe_3O_4 NPs was carried out a room temperature using a magnetic stirrer. First, a citrate salt solution was prepared. For this purpose, citrate salt (1.152 g, 6 mmol) by using magnetic stirring was dissolved in about 100 ml of deionized water. Then FeCl_3 (0.65 g, 4 mmol) and $\text{FeSO}_4 \cdot 7\text{H}_2\text{O}$ (0.56 g, 2 mmol) were added to the solution of citric acid and stirred with a magnetic stirrer at room temperature. Afterward, 3 ml of 25% ammonia solution was added under vigorous stirring. The prepared mixture was stirred for 1 h at 80 °C. Furthermore, the products could be purified by dialyzing them in deionized water for 5 times, during which the unreacted and residual ions were removed from the colloids. Finally, the ultrasmall Fe_3O_4 NPs were synthesized.

Preparation of $\text{Fe}_3\text{O}_4@$ FROP-1 NPs

For every 1 ml of the ultrasmall Fe_3O_4 NPs with a concentration of 3000 ppm, 0.5 mg of the peptide was added. Afterward, 1 ml of the ultrasmall Fe_3O_4 NPs synthesized in the previous step with a concentration of 3000 ppm, about 0.001 molecules of EDC, on the magnetic stirrer were added and stirred for 2 h at room temperature. The

final product was dialyzed 3 times in deionized water. This was done in the refrigerator.

Characterization techniques

Before using Fe_3O_4 and $\text{Fe}_3\text{O}_4@FROP-1$ NPs, their physicochemical properties were first evaluated by using different methods. At first, zeta potential and the effective diameters of NPs were measured by dynamic light scattering (DLS, Nano-flex, Germany). The morphology and size of the NPs were investigated by using transmission electron microscopy (TEM, Zeiss LEO 906, Germany) with a 120 kV accelerating voltage. To do this first, a small drop of the NP suspension diluted by deionized water was poured onto a carbon-coated grid, to evaporate and dry the liquid at room temperature and air temperature. Then, the network was monitored by TEM. In order to determine the type of bonding of peptide molecules at the nanoparticle surface, a Fourier transform infrared (FTIR) spectrometer (FTIR, Spectrum two Perkin Elmer, US). The iron content in different tissue samples were quantified by an inductively coupled plasma-mass spectrometer (ICP-MS, ELAN 6100 DRC-e, US). The structure of the synthesized NPs and the phases in the powder sample was determined by X-ray diffraction (XRD, Philips PW1730, UK) patterns. Measurements were collected with a Cu-K α radiation source and $\lambda = 1.540598 \text{ \AA}$ in the 2θ angle range with steps of 0.05° and 1 s/step . (Philips PW1730, UK). The structural analysis of elements in the sample and dispersive energy were investigated by energy-dispersive X-ray spectroscopy (EDX, FESEM-MIRA II, Czech Republic). The magnetic properties of pure Fe_3O_4 NPs were determined by a vibrating sample magnetometer (VSM, LBKFB, Lakeshore 7407, Iran) at room temperature.

Relaxivity measurements

In order to understand the MR efficiency and the relaxation rate of the Fe_3O_4 NPs, in vitro, we used two clinical 3T MRI scanner systems (Magnetom Prisma, Siemens, Germany). Therefore, a series of aqueous solutions of the Fe_3O_4 NPs at different Fe concentrations in 1.5 mL Eppendorf tubes were prepared. The spin-echo (SE) pulse sequence was used for the T1-weighted relaxation time, and the value of r_1 was calculated. The imaging parameters of the T1-weighted were as follows: Multiple Repetition Time (TR) = 100, 300, 600, 1200, 1800, 3000, 5000 ms, Echo Time (TE) = 12 ms, Number of Experiments = 7, Rare Factor = 2, Number of Repetitions = 1, Number of Averages = 1, Flip Angle = 180° , Matrix = 256×256 . The T2-weighted relaxation time was also performed using a multi-echo (ME) pulse sequence, and the value of r_2 was calculated. The imaging parameters of the T2-weighted were also selected as follows: Repetition Time (TR) = 2000 ms, Multiple Echo Time (TE) = 12, 24, 36, 48,

60, 72, 84, 96, 108, 120, 132, 144, 156, 168 ms, Number of Repetitions = 1, Number of Averages = 1, Flip Angle = 180° , Matrix = 256×256 , average = 10. The data was handled by Image J and MATLAB analyzed and obtained the T1 and T2 relaxation times for each sample. Then, the relaxivity values of r_1 and r_2 were calculated from the slope of the linear curve of inverse relaxation time ($1/T_1$ and $1/T_2$) vs. the Fe concentration (mM).

In vitro study

Cell culture

MCF-7, SKBR-3, MDA-MB-231 (human breast cancer adenocarcinoma), and MCF-10 (normal) cell lines were purchased from the Pasteur Institute of Iran (Tehran, Iran). The cell lines were cultured according to institutional guidelines with permission received from the Ethics Committee of Iran University of Medical Sciences (IUMS), in Dulbecco's Modified Eagle's Medium (DMEM) (Biowest, France) and supplemented with 10% fetal bovine serum (FBS) (GIBCO, New York, NY, USA) and 1% penicillin–streptomycin (Sigma-Aldrich, St. Louis, MO, USA). The cell lines were incubated in an incubator at 37°C with 5% CO_2 and saturation of moisture.

Cytotoxicity assay

The cell cytotoxicity of the Fe_3O_4 and $\text{Fe}_3\text{O}_4@FROP-1$ NPs was evaluated in MCF-7, SKBR-3, MDA-MB-231, and MCF-10 cell lines by using the 3-(4,5-dimethylthiazol-2-yl)-2,5-diphenyltetrazolium bromide (MTT) assay. MCF-7, SKBR-3, MDA-MB-231, and MCF-10 cell lines were seeded into 96-well culture plates with a density of 1×10^4 per well, and incubated in DMEM medium containing 10% FBS and 1% penicillin/streptomycin (pen/strep) under 5% CO_2 at 37°C for 24 h. Then, the medium was replaced with a fresh medium containing the Fe_3O_4 and $\text{Fe}_3\text{O}_4@FROP-1$ NPs at different Fe concentrations ($0 \sim 100 \mu\text{g/mL}$ NPs) in each well in 96-well plates. After 24 h, 20 μL of MTT (5 mg/mL in PBS) was added to the wells, and the cells were incubated for another 4 h under regular culture conditions. Afterward, the medium was carefully removed, and DMSO (200 μL) was added to each well to dissolve the formed formazan crystals. The absorbance at 570 and 630 nm in each well was measured with an ELISA reader (DANA-3200, Iran). The survival rate percentage of cells was calculated using the following Eq. (1):

$$\text{Cell Viability (\%)} = \frac{\text{Absorbance of treated group}}{\text{Absorbance of control group}} \times 100 \quad (1)$$

Cellular uptake of the Fe_3O_4 and $\text{Fe}_3\text{O}_4@FROP-1$ NPs

The specific cellular uptake in vitro studies of the Fe_3O_4 and $\text{Fe}_3\text{O}_4@FROP-1$ NPs by the MCF-7 cell line were first assessed by using an ICP-MS analysis. The MCF-7

cell line at a density of 3×10^5 cells/well was seeded in 6-well plates and grown to 80% confluency. After that, the medium was replaced with the medium containing the Fe_3O_4 and Fe_3O_4 @FROP-1 NPs with a Fe concentration of 0.5 mM. After incubation for 24 h, the wells were emptied and the cells were washed with PBS 2–3 times to remove any free NPs attached to the cell membrane. Then, the cells were trypsinized and centrifuged, and finally, the ICP-MS analysis was used to quantify the uptake of the Fe_3O_4 and Fe_3O_4 @FROP-1 NPs by cell lines.

Determination of specific binding

The saturation (blocking) method can be used to determine the effect of peptides attached to NPs. Using the saturation method, the selectivity of the peptide to the receptor can be investigated by blocking cell surface receptors with the free peptide. For this purpose, the MCF-7 cell line was first cultured. After reaching the appropriate cell density, to block cell surface receptors, the first 50 times the concentration of the peptide in Fe_3O_4 @FROP-1 NPs (0.5 mg/ml) of the free peptide were diluted in 3 ml of complete culture media. The cells were then incubated for 1 h with free peptide. After 1 h, the cells were washed twice with PBS solution. The cells were then treated with Fe_3O_4 @FROP-1 NPs at a concentration of 0.5 mM [Fe] and incubated for 24 h. 24 h after cell treatment, the cells were washed twice with PBS solution, trypsinized, and collected after centrifugation. The cell lines were immobilized in 1.5 mL tubes with 1% agarose.

T1-weighted MR imaging of the Fe_3O_4 and Fe_3O_4 @FROP-1 NPs

The in vitro T1-weighted MRI performance was compared by using the prepared Fe_3O_4 and Fe_3O_4 @FROP-1 NPs on the breast cancer cell lines; MCF-7, SKBR-3, MDA-MB-231, and MCF-10. MR images of the cell lines were obtained on an MRI scanner (3 Tesla). MCF-7, SKBR-3, MDA-MB-231, and MCF-10 cell lines were cultured in 6-well plates at a density of 1×10^5 cells/mL. MR images of the cell lines were collected after incubation with the Fe_3O_4 and Fe_3O_4 @FROP-1 NPs in the Fe concentration range (5, 10, 25, 50, and 100 $\mu\text{g}/\text{mL}$) for 24 h at 37 °C. After that, the cell lines were then washed twice with PBS, detached with trypsin, and then were centrifuged (5 min-1200 rpm). The acquired cell lines were resuspended in 0.2 mL agar gel solution (1%) in 1.5 mL Eppendorf tubes. The samples were prepared in 5 groups for the Fe_3O_4 and Fe_3O_4 @FROP-1 NPs. After preparing each group, we put it in a cold-water bath to seal the agar gel solution, and then it was transferred to the 4 °C refrigerator. Then, the MR images of the cell lines were taken. The imaging parameters were selected in such a way that it is possible to achieve the appropriate SNR and

resolution. The SNR and ΔSNR values were calculated by the following Eqs. (2) and (3), respectively:

$$\text{SNR} = \frac{\text{Signal Intensity (mean)}}{\text{Standard Deviation (noise)}} \quad (2)$$

$$\Delta\text{SNR} = \frac{\text{Signal Intensity (mean)} - \text{Signal Intensity (noise)}}{\text{Standard Deviation (noise)}} \times 100 \quad (3)$$

The T1-weighted MR images of the cell lines were acquired by using a conventional spin-echo sequence under the following parameters: echo time (TE)=14 ms, repetition time (TR)=800 ms, flip angle=120°, slice thickness=0.7 mm, number of excitations (NEX)=8, average=10.

Statistical analysis

All experiments were performed with three replications. Descriptive statistics of the studied variables were reported as the mean value \pm standard deviation (SD). Statistical significance was tested using an unpaired, two-tailed Student's t-test, assuming equal variance. Value of *($p < 0.05$), **($p < 0.01$), and ***($p < 0.001$) were considered to be statistically significant. Statistical differences for multiple groups were determined using a one-way ANOVA, and individual groups were compared using Student's t-tests. A p-value < 0.05 was considered statistically significant.

Results

Synthesis and characterization of the Fe_3O_4 and Fe_3O_4 @FROP-1 NPs

Herein, first the Fe_3O_4 and Fe_3O_4 @FROP-1 NPs were synthesized by the co-precipitation method. The hydrodynamic size of the Fe_3O_4 and Fe_3O_4 @FROP-1 NPs was measured to be 11.8 nm (Fig. 1a). The zeta potential was investigated and compared before and after binding of FROP-1 peptide to Fe_3O_4 NPs. The zeta potential of the NPs was -40.28 ± 4.80 mV before binding to the peptide and -30 ± 3 after binding to the peptide, indicating the high stability of the NPs (Fig. 1b).

In order to investigate the morphology and size of NPs, TEM images were prepared, which are shown in Fig. 1c. The Fe_3O_4 NPs have a spherical or quasi-spherical shape with a relatively uniform size distribution. The mean diameters of the Fe_3O_4 NPs were measured at 3.78 ± 0.2 nm. FTIR spectrometer was used to determine the type of bonding of peptide molecules at the NP surface by using the attenuated total reflectance (ATR) method from 4000 to 400 cm^{-1} . As shown in Fig. 1d, the presence of the Fe_3O_4 nuclei is characterized by strong tensile adsorption at 579 cm^{-1} , which is related to Fe-O bonding. The presence of a peak in the

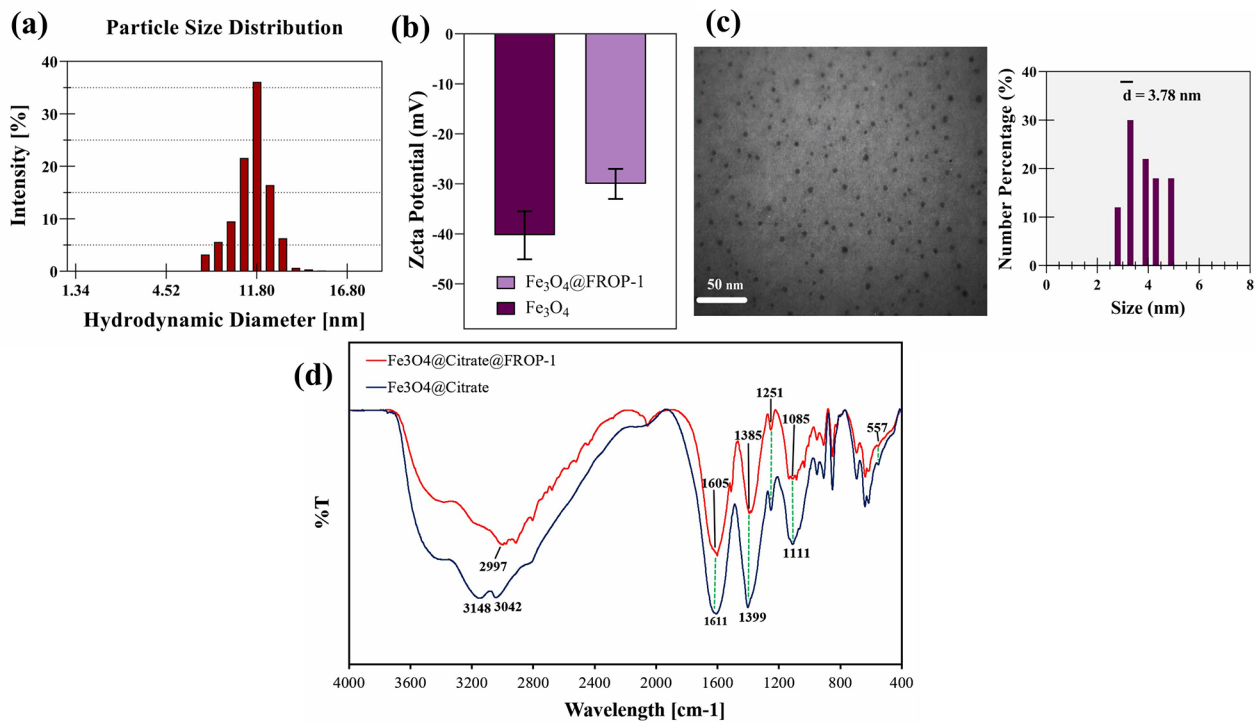


Fig. 1 (a) DLS data of Fe_3O_4 NPs in water; (b) Zeta potential of Fe_3O_4 and Fe_3O_4 @ FROP-1 NPs; (c) TEM image of Fe_3O_4 NPs, and; (d) FTIR spectroscopy of Fe_3O_4 and Fe_3O_4 @ FROP-1 NPs

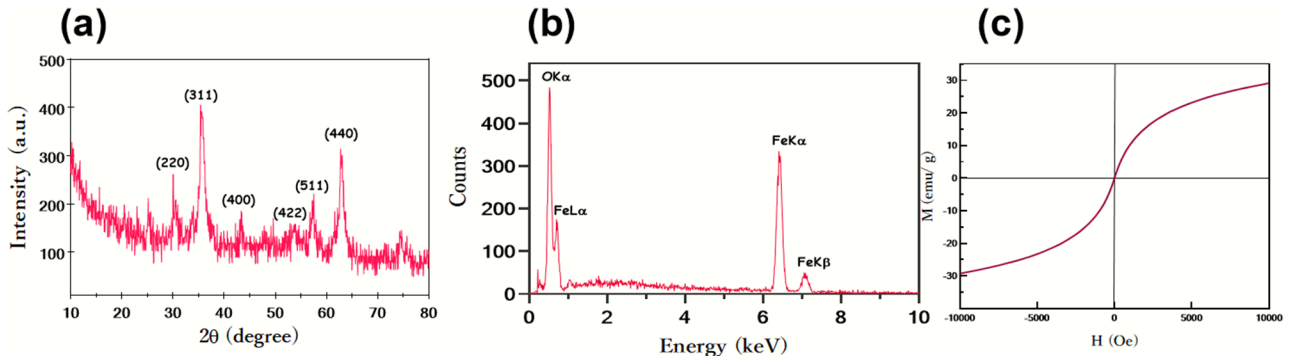


Fig. 2 (a) XRD; (b) EDX and; (c) magnetization curves of Fe_3O_4 NPs

region of 557 cm^{-1} in the resulting spectrum confirms the presence of magnetite NPs. The peak of the carbonyl citrate group appeared above 1700 cm^{-1} , while the peak of the carbonyl citrate group attached to the surface of the magnetite NP appeared at 1611 cm^{-1} . This indicates displacement due to interaction and complex formation with magnetite NPs. Binding of the amine of the FROP-1 peptide to the carboxyl group on the NP surface results in the formation of an amide group that appears at 1605 cm^{-1} [21].

The structure of the synthesized NPs and the phases in the powder sample were determined by the X-ray diffraction pattern. As shown by XRD patterns obtained using (Fig. 2a). The peaks visible at the Bragg angles of

$2\theta \sim 30.1^\circ, 35.51^\circ, 43.1^\circ, 53.11^\circ, 57.01^\circ,$ and 62.56° respectively represent the crystalline planes (220), (311), (400), (422), (511), and (440) and according to JCPDS card no. 19-0629, Fe_3O_4 iron oxide NPs have a complete crystal structure and no impurity peak is observed in them. This confirms the magnetic nature of Fe_3O_4 NPs [22]. Besides, the elements in the NPs were analyzed using EDX energy diffraction spectroscopy. In the EDX spectrum of the NPs in Fig. 2b, the peaks appearing at 0.60, 0.70, 6.41, and 7.06 kV (keV) correspond to the binding energies of O and Fe, indicating the presence of iron in the NPs. The magnetic properties of the Fe_3O_4 NPs were investigated by VSM analysis, and it shows the magnetization 'M' versus the applied field 'H' (between -10 and $+10\text{ kOe}$) of

the prepared Fe_3O_4 NPs at room temperature. As shown in Fig. 2c, the saturation magnet (M_s) of the Fe_3O_4 NPs is 29 emu/g. The results indicate that Fe_3O_4 with 29 emu/g is one of the best options for biomedical applications.

Relaxivity measurements

In the present study, we synthesized Fe_3O_4 in different Fe concentrations and investigated the potential to use them as T1w MRI contrast agents (Fig. 2). The T1w MR images of the Fe_3O_4 in different Fe concentrations are shown in Fig. 3a. Figure 3b, c shows the plots of $1/T_1$ and $1/T_2$ as a function of Fe concentration. The slopes of the $1/T_1$ and $1/T_2$ plots determine the longitudinal and transverse relaxivities (r_1 and r_2), respectively. Therefore, the values of r_1 and r_2 were calculated for Fe_3O_4 and Dotarem (gadoterate meglumine). As shown, the r_1 values of the Fe_3O_4 NPs and Dotarem were obtained to be 2.608 and $3.036 \text{ mM}^{-1}\text{s}^{-1}$, respectively, and the r_2/r_1 ratios were 1.18 and 1.3 respectively. The low r_2/r_1 ratio values showed that the synthesized Fe_3O_4 NPs had strong T1-weighted relaxation properties, and could be used as T1w contrast agents. Figure 3d, e shows that

with an increasing Fe concentration in the samples, the signal intensity increases. The results demonstrated that synthesized NPs have better imaging performance than Dotarem.

In vitro cytotoxicity assay

The cytotoxicity of the Fe_3O_4 and Fe_3O_4 @FROP-1 NPs, was evaluated using MTT assay, and the cell survival rate of the cell lines was determined. Herein, the toxicity of the Fe_3O_4 and Fe_3O_4 @FROP-1 NPs on different MCF-7, SKBR-3, MDA-MB-231, and MCF-10 cell lines as well as at different concentrations (0–2 mM) for 24 h was investigated. Figure 4 compares the viability of treated cell lines with the Fe_3O_4 and Fe_3O_4 @FROP-1 NPs after 24 h of post-treatment. Cell survival decreases with the increasing concentration of NPs. Both of the Fe_3O_4 and Fe_3O_4 @FROP-1 NPs showed little cytotoxicity. We clearly observe that at the tested highest Fe concentration (2 mM) used in this study, the cell lines treated with the Fe_3O_4 and Fe_3O_4 @FROP-1 NPs show quite high survival, about 70%. These results indicate that both the Fe_3O_4 and Fe_3O_4 @FROP-1 NPs have good cytocompatibility in the

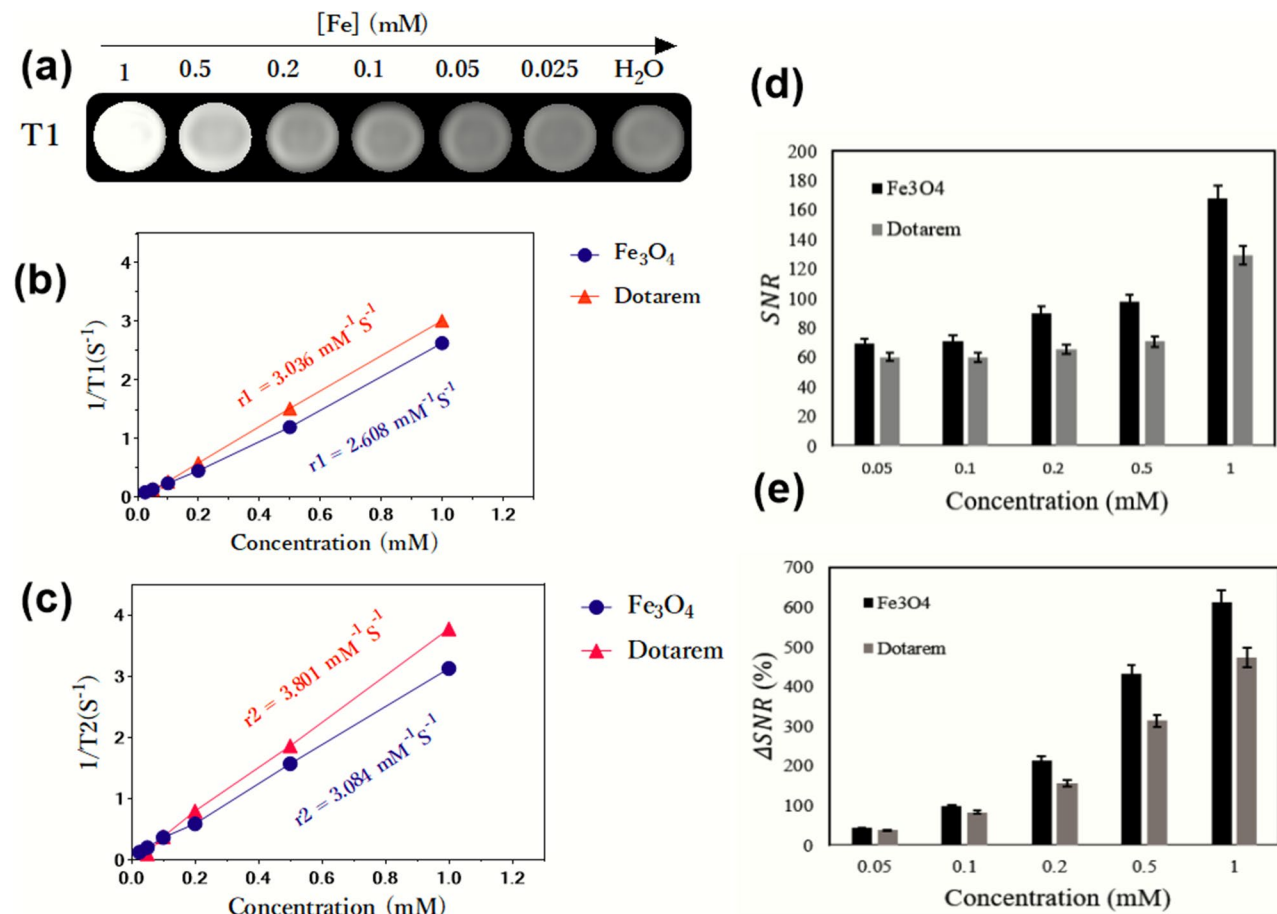


Fig. 3 (a) T1-weighted MR images of the Fe_3O_4 NPs; (b) r_1 and; (c) r_2 relaxivity values of the Fe_3O_4 NPs and Dotarem; (d) relative MR SNR of Fe_3O_4 and Dotarem at different Fe concentrations in water and at 3T MR system

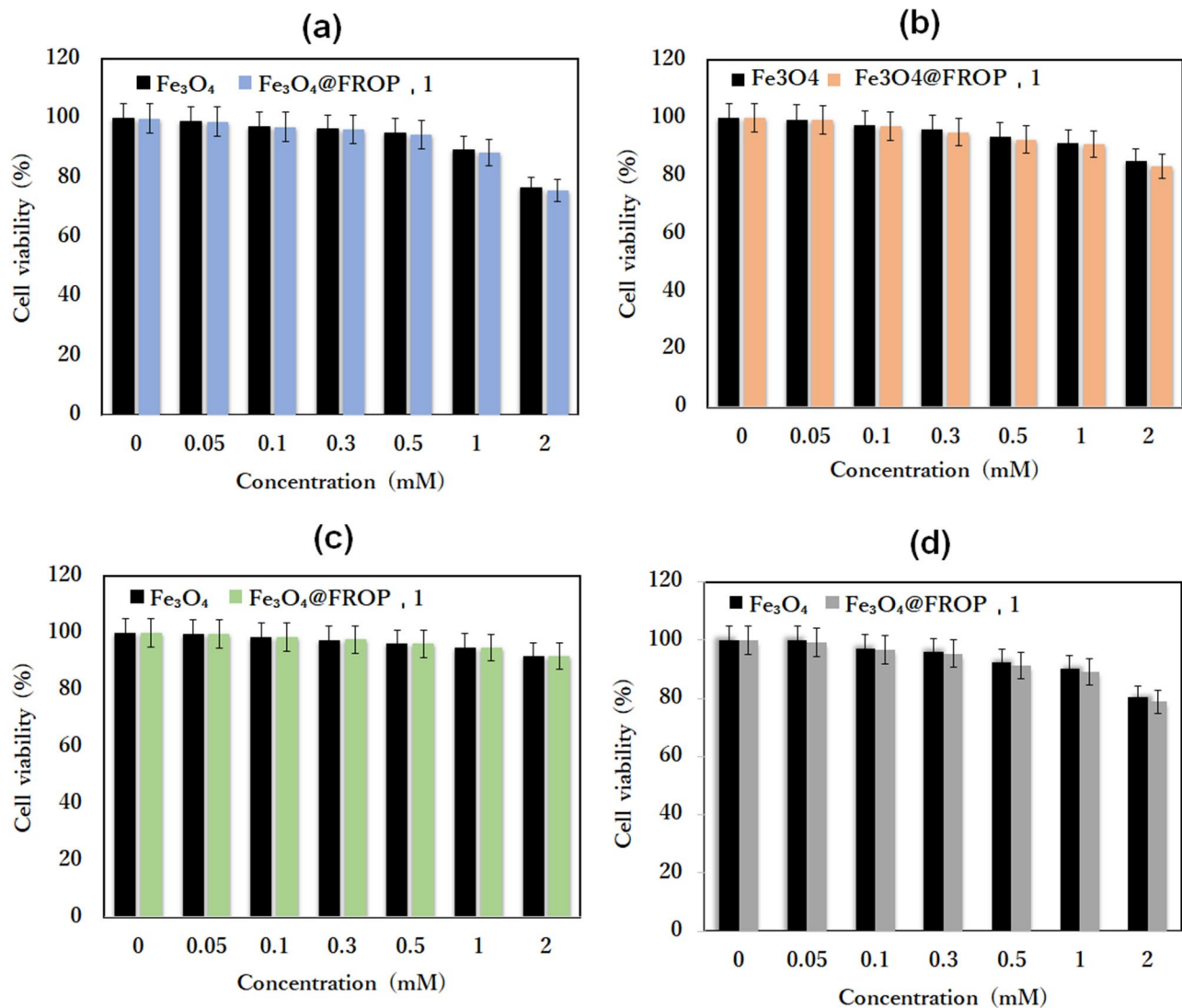


Fig. 4 Cell viability of (a) MCF-7; (b) SKBR-3; (c) MDA-MB-231 and; (d) MCF-10 cell lines incubated with the Fe₃O₄ and; (b) Fe₃O₄@FROP-1 NPs in different concentrations (0/control, 0.05, 0.1, 0.3, 0.5, 1, and 2 mM) at 24 h at 37 °C ($n=8, p<0.05$)

studied concentration range. This study showed that the Fe₃O₄ and Fe₃O₄@FROP-1 NPs had almost no toxicity at concentrations less than 0.5 mM after incubation for 24 h (about 99% and 91% viability, respectively; $P<0.05, n=8$).

The cellular uptake of the Fe₃O₄ and Fe₃O₄@FROP-1 NPs

ICP-MS was used to assess the cellular uptake of the Fe₃O₄ and Fe₃O₄@FROP-1 NPs and also to measure the Fe concentrations in the MCF-7 cell line (Fig. 5a). For this purpose, the MCF-7 cell line was incubated with the Fe₃O₄ and Fe₃O₄@FROP-1 NPs, at a concentration of 0.5 mM for 24 h to compare the Fe concentration in the cell lines after cellular uptake. The ICP-MS studies revealed that the Fe uptake of Fe₃O₄@FROP-1 in the MCF-7 cell line was about 1.6 times greater than that of the Fe₃O₄ NPs. Fe₃O₄@FROP-1 NPs showed higher cellular uptake than the Fe₃O₄ NPs by the MCF-7 cell line. This was

caused by the capability of the FROP-1 peptide conjugated Fe₃O₄ NPs to bind to the MCF-7 cell line, increasing cellular internalization. This accumulation effect could account for the higher concentration of Fe in the MCF-7 cell line when the Fe₃O₄ and Fe₃O₄@FROP-1 NPs were internalized by the cells. These results indicate that the FROP-1 peptide conjugated to the Fe₃O₄ NPs has a significant effect on cellular uptake efficiency.

Determination of specific binding of the Fe₃O₄@FROP-1 NPs

The ability to bind the Fe₃O₄@FROP-1 NPs by saturation test was demonstrated on MCF-7 cells. As shown in Fig. 5b MCF-7 cells blocked with free FROP-1 peptide showed less signal intensity than the cells that were unblocked.

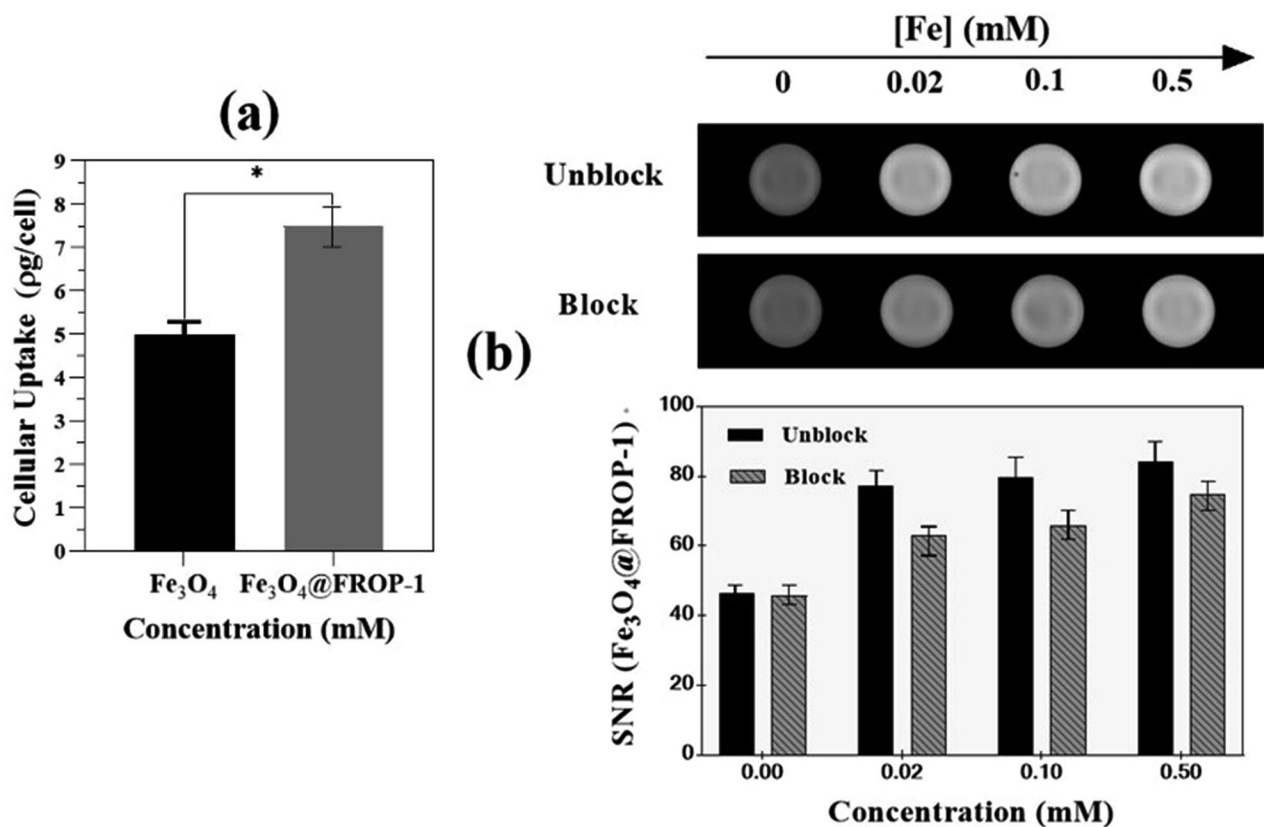


Fig. 5 Cellular uptake of the (a) Fe₃O₄ and; (b) Fe₃O₄@FROP-1 NPs in MCF-7 cell line as analyzed by ICP-MS

Targeted T1-weighted MR imaging of cell lines

To validate the MRI performance of the Fe₃O₄ and Fe₃O₄@FROP-1 NPs, different concentrations of samples from 0 to 100 µg/mL were used to incubate the MCF-7, SKBR-3, MDA-MB-231, and MCF-10 cell lines for 24 h. Then, the T1w MR images of the Fe₃O₄ and Fe₃O₄@FROP-1 NPs were carried out at different Fe concentrations at 3T, and the corresponding signal intensity value of the cell lines was measured. As is clear from the T1w MR images (Fig. 6), the Fe₃O₄ and Fe₃O₄@FROP-1 NPs show increased MR signal intensity with the Fe concentration. The contrast enhancement was obtained by using Eqs. (2) and (3). The changes in the signal intensity at different concentrations of iron (0~100 µg/ml) were significant. In other words, the MRI signal intensity of the MCF-7 cell line treated with Fe₃O₄ NPs decreased more significantly than Fe₃O₄@FROP-1 NPs (p-value < 0.05) (Fig. 7). Based on the results, it can be stated that Fe₃O₄@FROP-1 NPs as a targeted T1 contrast agent have a high potential for the diagnosis of breast cancer in vitro.

Discussion

Breast cancer remains a major global health challenge, with early and accurate detection playing a crucial role in improving survival rates. The global pandemic of the coronavirus in 2019 affected all medical infrastructure in

such a way that the World Health Organization (WHO) announced in 2021 that breast cancer has for the first-time surpassed lung cancer as the most common cancer in the world, highlighting the urgent need for early and accurate diagnostic strategies [23–25]. Considering the importance of early detection of breast cancer, the use of targeted imaging methods such as MRI plays an important role in the non-invasive diagnosis of tumors in the early stages, as well as the selection of more effective treatment methods. MRI has become one of the most powerful and widely used diagnostic tools due to its high spatial resolution, non-use of ionizing radiation, and non-invasiveness and can be a more suitable alternative to mammography [26–28]. But the early and accurate detection of breast cancer in MR imaging systems requires the development of contrast agents with the ability to target the cancer cells so that, with specific distribution, they can potentially provide effective detectable contrast in small tumors and micrometastases [17, 21]. Traditional GBCAs are widely used in MRI; however, they present significant challenges, including potential toxicity, nephrogenic systemic fibrosis, and gadolinium deposition in the brain [11, 13, 14]. These limitations highlight the need for safer, tumor-specific alternatives with enhanced specificity and imaging accuracy. SPIONs

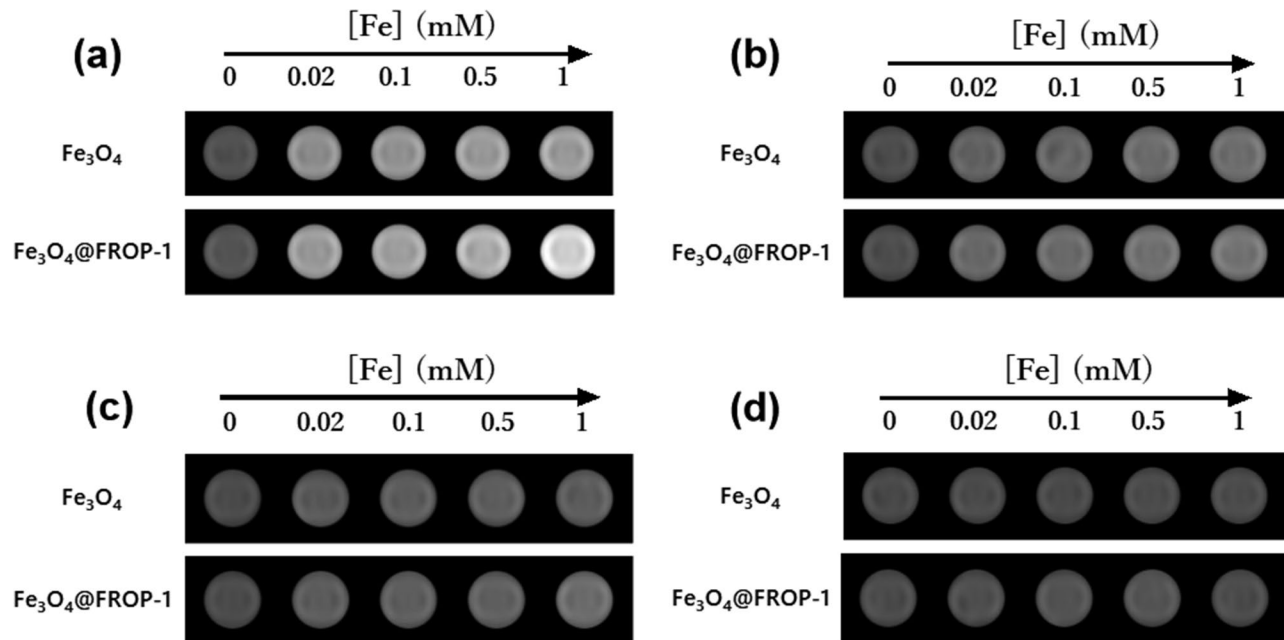


Fig. 6 A complete T1w MR images of the (a) MCF-7; (b) SKBR-3; (c) MDA-MB-231 and; (d) MCF-10 cell lines that were treated with various Fe concentrations of the Fe_3O_4 and $\text{Fe}_3\text{O}_4@FROP-1$ NPs

NPs have emerged as promising MRI contrast agents, but their predominant T2 effects often limit their application in T1-weighted imaging.

So far, many studies have been conducted on the effect of NPs size on the magnetic properties of MR contrast agents. These studies show that in USPIO NPs (<5 nm), as the size of the NPs decreases, their magnetic moment decreases rapidly, and this can inhibit the T2 relaxation effect while enhancing T1 relaxivity, making them more suitable for T1-weighted MRI. Therefore, it seems that the size of magnetic NPs has a decisive role in the relaxation time of protons and relaxivity parameters. Also, due to the small size of these particles, they are not easily recognized by phagocytes, have a longer half-life, and can be used as targeted delivery systems [29, 30]. In this study USPIO NPs conjugated with the FROP-1 peptide were used as targeted T1 contrast agents in MR imaging in vitro. The USPIO NPs were synthesized using the co-precipitation method. Then, sodium citrate-stabilized Fe_3O_4 NPs were conjugated with the FROP-1 peptide by EDC and they were investigated using different characterization techniques. The results of the characterization techniques confirmed that the synthesized USPIO NPs are almost spherical and 3.78 ± 0.2 nm in size. Our results demonstrate that $\text{Fe}_3\text{O}_4@FROP-1$ NPs effectively function as a T1 contrast agent, as indicated by an $r2/r1$ ratio of 1.18, which falls within the optimal range for T1 agents ($r2/r1 < 5$). This is a significant advantage over traditional SPION-based contrast agents, which typically exhibit strong T2 effects. Moreover, the results of ICP-MS analysis revealed a 1.6-fold increase in cellular uptake of

$\text{Fe}_3\text{O}_4@FROP-1$ NPs compared to non-targeted USPIOs in MCF-7 breast cancer cells, confirming their enhanced targeting capability. This increased uptake correlates with a significant improvement in T1-weighted MRI signal intensity, demonstrating the potential of these nanoparticles as effective tumor-targeted contrast agents.

The FROP-1 peptide, which consists of 12-amino-acids with the sequence Glu-Asn-Tyr-Glu-Leu-Met-Asp-Leu-Leu-Ala-Tyr-Leu, in 2007 by Zitzmann et al. by using phage display system was identified to target different types of cancer cell lines. This research demonstrated that the FROP-1 peptide labeled with ^{131}I and ^{125}I radionuclides can specifically bind to MCF-7 breast tumor cells both in vitro and in vivo [18]. In 2018, studies on the specific binding ability of the FROP-1 peptide to MCF-7 cells in vitro and in vivo were developed and continued. Ahmadpour et al. found that the FROP-1 peptide labeled with $^{99\text{m}}\text{Tc}$ radionuclide with the highest uptake of MCF-7 cells in breast cancer has the potential to be used in early tumor diagnosis [19]. Previous studies have successfully radiolabeled this peptide with ^{131}I , ^{125}I , and $^{99\text{m}}\text{Tc}$ for targeted imaging applications, demonstrating its strong affinity for MCF-7 breast cancer cells in both in vitro and in vivo studies. However, its potential as an MRI contrast agent had not been explored before this study. Given the importance of this issue, this peptide could be a good choice as a targeted contrast agent for targeting breast tumors in MRI imaging.

Our findings confirm that the studied NPs exhibit high stability, good biocompatibility, and significant cellular uptake in breast cancer cells.

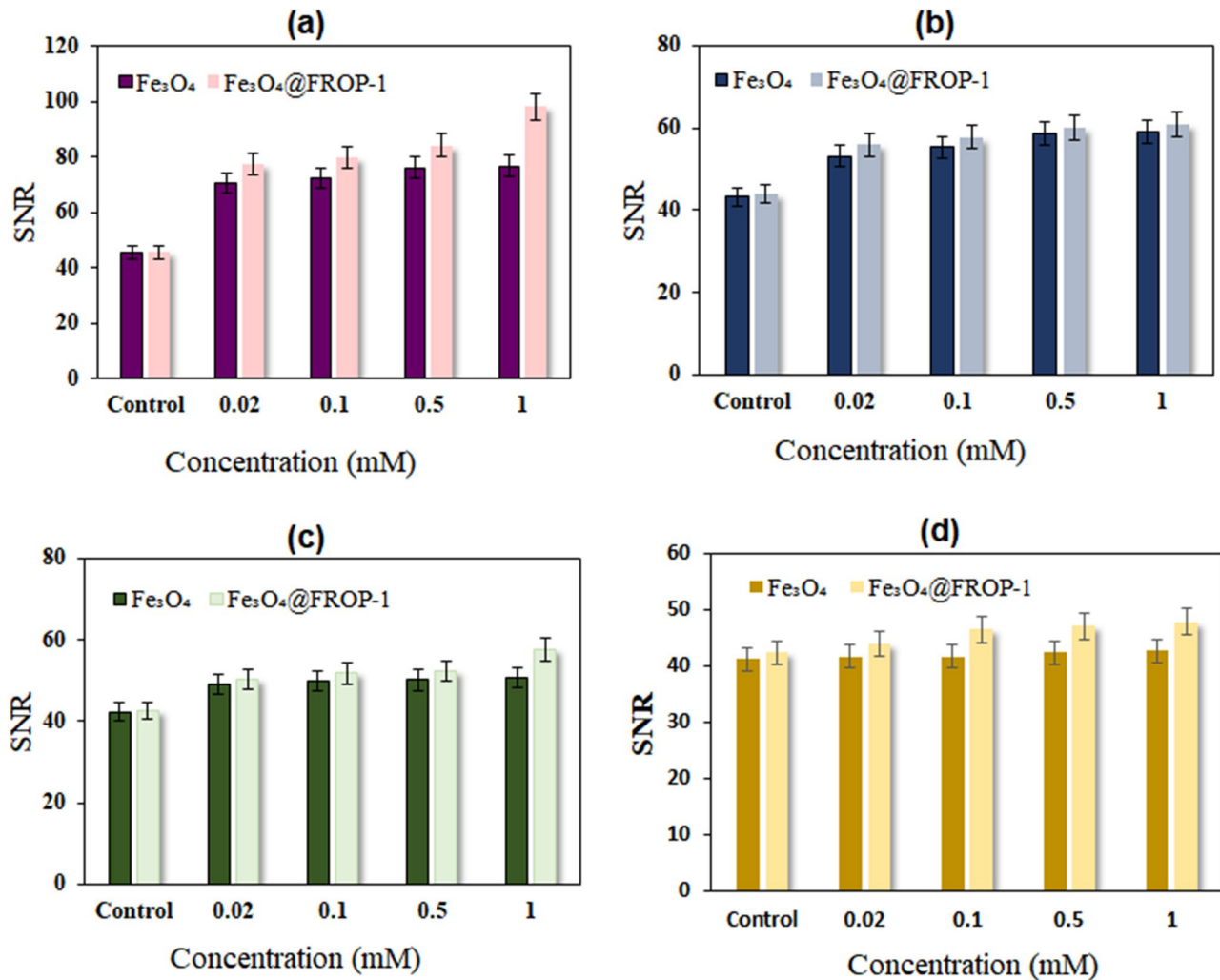


Fig. 7 Comparison of SNR plots for the (a) MCF-7; (b) SKBR-3; (c) MDA-MB-231 and; (d) MCF-10 cell lines that were treated with various Fe concentrations of the Fe_3O_4 and $\text{Fe}_3\text{O}_4@FROP-1$ NPs

One of the parameters affecting MRI image quality is the signal-to-noise ratio (SNR) [31]. T1w images of breast cancer cell lines showed that the SNR of cells treated with $\text{Fe}_3\text{O}_4@FROP-1$ NPs was significantly higher. Furthermore, the results of the saturation method indicate that $\text{Fe}_3\text{O}_4@FROP-1$ NPs have the ability to specifically target cell surface receptors.

Given the biocompatibility, stability, and tumor-targeting properties of $\text{Fe}_3\text{O}_4@FROP-1$ NPs, they hold strong potential for clinical translation as an alternative to conventional contrast agents. Moreover, the ability to functionalize these nanoparticles with additional ligands or therapeutic agents opens avenues for multimodal imaging and theranostic applications.

Conclusion

In summary, this study evaluated the performance of $\text{Fe}_3\text{O}_4@FROP-1$ NPs as a novel targeted MRI contrast agent for in vitro imaging of breast cancer cells.

The obtained data confirmed that the synthesized the Fe_3O_4 NPs were almost spherical, with an average size of 3.78 ± 0.2 nm. Furthermore, the cytotoxicity assay results in the studied Fe concentration range showed good biocompatibility. The obtained longitudinal relaxivity (r_1) and r_2/r_1 ratio (1.18) indicate that these NPs have a high potential as effective T1 contrast agents in diagnostic MR imaging of breast cancer in vitro.

Their small size, high r_1 relaxivity, and tumor-targeting capability make them a promising alternative to traditional GBCAs and untargeted SPION-based contrast agents.

Considering their promising in vitro performance, further in vivo investigations are warranted to assess their pharmacokinetics, biodistribution, and imaging efficacy in preclinical models. Additionally, functionalizing $\text{Fe}_3\text{O}_4@FROP-1$ NPs with other ligands or therapeutic agents could expand their potential applications in multimodal imaging and targeted therapy. These findings

highlight the potential of Fe₃O₄@FROP-1 NPs as theranostic multifunctional nanopatforms for precision cancer diagnostics and treatment.

Abbreviations

DLS	Dynamic light scattering
EDC	1-Ethyl-3-(3-dimethylaminopropyl)carbodiimide
EDTA	Ethylene diamine tetra-acetic acid
FTIR	Fourier transform infrared spectroscopy
GBCAs	Gadolinium-based contrast agents
ICP-MS	Inductively coupled plasma mass spectrometry
MRI	Magnetic resonance imaging
MTT	3-(4,5-dimethylthiazol-2-yl)-2,5-diphenyltetrazolium bromide
PBS	Phosphate buffered saline
ROI	Region of interest
ROS	Reactive oxygen species
SNR	Signal-to-noise ratio
TEM	Transmission electron microscope
USPIO	Ultrasmall superparamagnetic iron oxide

Acknowledgements

Not applicable.

Author contributions

MS, SK, and HG contributed to the study conception and design. HG contributed to material preparation. RI performed nanoparticle synthesis and characterization. VP performed TEM study. MS, ZA, RI, and AS conducted the experiments and collected the data. MS performed data analysis and drafted the first of the manuscript. All the authors reviewed the manuscript. All aspects of the study were supervised by HG and SK.

Funding

This work was supported by Zahedan University of Medical Sciences (grant No. 7970) and Iran University of Medical Sciences (grant No. 13419).

Data availability

The datasets used and/or analyzed during the current study are available from the corresponding author on reasonable request.

Declarations

Ethics approval and consent to participate

This research was approved by Ethics Committee of Iran University of Medical Sciences.

Consent to participate

Not applicable.

Competing interests

The authors declare no competing interests.

Author details

¹Finetech in Medicine Research Center, Iran University of Medical Sciences, Tehran, Iran

²Medical Physics Department, Iran University of Medical Sciences, Tehran, Iran

³Neuroscience Research Center, Iran University of Medical Sciences, Tehran, Iran

⁴Pharmacology Research Center, Zahedan University of Medical Sciences, Zahedan, Iran

Received: 15 December 2024 / Accepted: 2 April 2025

Published online: 01 May 2025

References

- Han Z, Wu X, Roelle S, Chen C, Schiemann WP, Lu Z-RJN. Targeted Gadofullerene for sensitive magnetic resonance imaging and risk-stratification of breast cancer. *Nat Commun*. 2017;8(1):692.
- Wang G, Gao W, Zhang X, Mei X. Au nanocage functionalized with Ultra-small Fe₃O₄ nanoparticles for targeting T1-T2 dual MRI and CT imaging of tumor. *J Sci Rep*. 2016;6(1):1–10.
- Shi Z, Huang X, Cheng Z, Xu Z, Lin H, Liu C, et al. MRI-based quantification of intratumoral heterogeneity for predicting treatment response to neoadjuvant chemotherapy in breast cancer. *Radiology*. 2023;308(1):e222830.
- Obayemi J, Salifu A, Eluu S, Uzonwanne V, Jusu S, Nwazojie C et al. LHRH-conjugated drugs as targeted therapeutic agents for the specific targeting and localized treatment of triple negative breast cancer. 2020;10(1):1–18.
- Luo Y, Yang J, Yan Y, Li J, Shen M, Zhang G, et al. RGD-functionalized ultrasmall iron oxide nanoparticles for targeted T1-weighted MR imaging of gliomas. *Nanoscale*. 2015;7(34):14538–46.
- Xie J, Chen K, Lee H-Y, Xu C, Hsu AR, Peng S, et al. Ultrasmall C (RGDyK)-coated Fe₃O₄ nanoparticles and their specific targeting to integrin $\alpha v\beta 3$ -rich tumor cells. *J Am Chem Soc*. 2008;130(24):7542–3.
- Bai C, Jia Z, Song L, Zhang W, Chen Y, Zang F, et al. Time-Dependent T1-T2 switchable magnetic resonance imaging realized by C (RGDyK) modified ultrasmall Fe₃O₄ nanoprob. *Adv Funct Mater*. 2018;28(32):1802281.
- Shin T-H, Kim PK, Kang S, Cheong J, Kim S, Lim Y, et al. High-resolution T1 MRI via renally clearable dextran nanoparticles with an iron oxide shell. *J Nat Biomedical Eng*. 2021;5(3):252–63.
- Yin J, Yin G, Pu X, Huang Z, Yao DJRA. Preparation and characterization of peptide modified ultrasmall superparamagnetic iron oxides used as tumor targeting MRI contrast agent. *RSC Adv*. 2019;9(34):19397–407.
- Fernández-Barahona I, Muñoz-Hernando M, Ruiz-Cabello J, Herranz F, Pellico JJI. Iron oxide nanoparticles: an alternative for positive contrast in magnetic resonance imaging. *Inorganics*. 2020;8(4):28.
- Vangjizzegem T, Stanicki D, Boutry S, Paternoster Q, Vander Elst L, Muller R, Laurent SJN. VSION as high field MRI T1 contrast agent: evidence of their potential as positive contrast agent for magnetic resonance angiography. *Nanotechnology*. 2018;29(26):265103.
- Xiang C, Zhong X, Yang W, Majeed MI, Wang J, Yu J, et al. Fe₃O₄ nanoparticles functionalized with polymer ligand for T1-Weighted MRI in vitro and in vivo. *Polymers*. 2019;11(5):882.
- An L, Cai Y, Tian Q, Lin J, Yang S. Ultrasensitive iron-based magnetic resonance contrast agent constructed with natural polyphenol Tannic acid for tumor theranostics. *J Sci China Mater*. 2021;64(2):498–509.
- Jafari A, Salouti M, Shayesteh SF, Heidari Z, Rajabi AB, Boustani K, Nahardani AJN. Synthesis and characterization of Bombesin-superparamagnetic iron oxide nanoparticles as a targeted contrast agent for imaging of breast cancer using MRI. *Nanotechnology*. 2015;26(7):075101.
- Wang H, Jiang Q, Shen Y, Zhang L, Haacke EM, Ge Y, et al. The capability of detecting small vessels beyond the conventional MRI sensitivity using iron-based contrast agent enhanced susceptibility weighted imaging. *J NMR Biomed*. 2020;33(5):e4256.
- Wang C, Yan C, An L, Zhao H, Song S, Yang S. Fe₃O₄ assembly for tumor accurate diagnosis by endogenous GSH responsive T2/T1 magnetic relaxation conversion. *J Mater Chem B*. 2021.
- Accardo A, Tesaro D, Morelli GJP. Peptide-based targeting strategies for simultaneous imaging and therapy with nanovectors. *Polym J*. 2013;45(5):481–93.
- Zitzmann S, Krämer S, Mier W, Hebling U, Altmann A, Rother A, et al. Identification and evaluation of a new tumor Cell-Binding peptide, FROP-1. *J Nucl Med*. 2007;48(6):965–72.
- Ahmadpour S, Noaparast Z, Abedi SM, Hosseini-mehr SJJ. 99m Tc-HYNIC-(tricine/EDDA)-FROP peptide for MCF-7 breast tumor targeting and imaging. *J Biomed Sci*. 2018;25(1):17.
- Mier W, Zitzmann S, Krämer S, Reed J, Knapp E-M, Altmann A, et al. Influence of chelate conjugation on a newly identified tumor-targeting peptide. *J Nucl Med*. 2007;48(9):1545–52.
- Shen J-M, Li X-X, Fan L-L, Zhou X, Han J-M, Jia M-K, et al. Heterogeneous dimer peptide-conjugated polylysine dendrimer-Fe₃O₄ composite as a novel nanoscale molecular probe for early diagnosis and therapy in hepatocellular carcinoma. *Int J Nanomed*. 2017;12:1183.
- Sheng S, Liu W, Zhu K, Cheng K, Ye K, Wang G, et al. Fe₃O₄ nanospheres in situ decorated graphene as high-performance anode for asymmetric supercapacitor with impressive energy density. *J Colloid Interface Sci*. 2019;536:235–44.
- Li X, Fan Z, Jiang H, Niu J, Bian W, Wang C, et al. Synthetic MRI in breast cancer: differentiating benign from malignant lesions and predicting immunohistochemical expression status. *Sci Rep*. 2023;13(1):17978.

24. Wilke LG, Nguyen TT, Yang Q, Hanlon BM, Wagner KA, Strickland P et al. Analysis of the impact of the COVID-19 pandemic on the multidisciplinary management of breast cancer: review from the American society of breast surgeons COVID-19 and mastery registries. *Ann Surg Oncol*. 2021;1–9.
25. Siegel RL, Miller KD, Wagle NS, Jemal A. Cancer statistics, 2023. *Cancer J Clin*. 2023;73(1):17–48.
26. Ozturk MS, Montero MG, Wang L, Chaible LM, Jechlinger M, Prevedel R. Intra-vital mesoscopic fluorescence molecular tomography allows non-invasive in vivo monitoring and quantification of breast cancer growth dynamics. *J Commun Biology*. 2021;4(1):1–11.
27. Zhou Z, Qutaish M, Han Z, Schur RM, Liu Y, Wilson DL, Lu Z-RJN. MRI detection of breast cancer micrometastases with a fibronectin-targeting contrast agent. *Nat Commun*. 2015;6(1):1–11.
28. Saslow D, Boetes C, Burke W, Harms S, Leach MO, Lehman CD, et al. American cancer society guidelines for breast screening with MRI as an adjunct to mammography. *J CA: cancer J Clin*. 2007;57(2):75–89.
29. Zhao X, Zhao H, Chen Z, Lan M. Ultrasmall superparamagnetic iron oxide nanoparticles for magnetic resonance imaging contrast agent. *J Nanosci Nanotechnol*. 2014;14(1):210–20.
30. Chen C, Ge J, Gao Y, Chen L, Cui J, Zeng J, Gao M. Ultrasmall superparamagnetic iron oxide nanoparticles: A next generation contrast agent for magnetic resonance imaging. *Wiley Interdisciplinary Reviews: Nanomed Nanobiotechnol*. 2022;14(1):e1740.
31. Shokrollahi P, Drake JM, Goldenberg AAJB. Signal-to-noise ratio evaluation of magnetic resonance images in the presence of an ultrasonic motor. *Biomed Eng Online*. 2017;16(1):1–12.

Publisher's note

Springer Nature remains neutral with regard to jurisdictional claims in published maps and institutional affiliations.